Adsorption of reactive green 19 from water using polyaniline/bentonite

Jingxi Tie, Dongguang Chen, Meiqi Zhao, Xiaolei Wang, Shangang Zhou and Longgui Peng

ABSTRACT

Polyaniline/bentonite was used in this study to investigate its adsorption behaviors of reactive green 19. Influencing factors including contact time, pH, temperature and inorganic salts were investigated. The adsorption kinetic data fitted the pseudo-second-order model better than the pseudo-first-order and Elovich models, and the Langmuir model was better than the Freundlich model to describe the adsorption process. Thermodynamic studies indicated that the adsorption of reactive green 19 by polyaniline/bentonite was an endothermic and spontaneous process. Experimental data indicated that both NaCl and Na_2SO_4 could improve the reactive green 19 adsorption as a result of aggregation of the dye molecules in solution induced by the inorganic salts, and an increase of pH value from 5 to 9 caused a slight decrease in reactive green 19 adsorption.

Key words | adsorption, isotherm, kinetics, polyaniline/bentonite, reactive green 19, thermodynamics

Jingxi Tie
Dongguang Chen
Xiaolei Wang
Shangang Zhou
School of Environmental and Municipal Engineering,
North China University of Water Resources and Electric Power,
Zhengzhou, 450011, China

Jingxi Tie
School of Environmental Science and Engineering,
Nanjing University of Information Science and Technology,
Nanjing, 210044, China

Meiqi Zhao
College of Environment,
Hehai University,
Nanjing, 210044, China

Longgui Peng (corresponding author)
School of Materials Science and Engineering,
Xi'An University of Science and Technology,
Xi'an 710054, China
E-mail: *1840655607@qq.com*

INTRODUCTION

China produced approximately two-thirds of the total global textile fibers in 2012, ranking in the top three largest textile manufacturers worldwide (Peng *et al.* 2015). Hence, large quantities of dyes have to be generated to meet the needs of the textile production. At present, China is the largest producer of dyes in the world. Data from the China Dyestuff Industry Association (CDIA) show that the annual production of commercial dyes was 8.95×10^5 tons in 2013, accounting for about 65% of the world yield. The huge dye applications have attracted increasing public concern because about 30% of the used dyestuffs are lost during dyeing processes, to generate large volumes of dye-bearing effluents with high concentrations of dyes. The total discharge of dyeing wastewater was 1.96×10^9 m^3 in 2013 in China (Wang *et al.* 2015a, 2015b). The organics, bleaches and salts in dyeing effluents can not only cause deterioration of the quality of receiving water bodies, but can also destroy the aquatic ecosystems and even cause serious health issues since some dyes or their degradation intermediates are cancerogenic, teratogenic and mutagenic (Gong *et al.* 2009; Tang *et al.* 2014). However, the chemical stability resulting from their mainly aromatic structures makes the dyes resistant to traditional biodegradation (Ewa & Gra 2007; Wang & Wang 2008). Therefore, physicochemical techniques including adsorption, ozonation, nanofiltration, coagulation and photocatalytic oxidation etc. have been developed to treat dye-containing effluents (Mahmoodi 2013; Ong *et al.* 2013; Zhang *et al.* 2013; Liang *et al.* 2014; Rosa *et al.* 2014; Hua *et al.* 2015; Kim *et al.* 2015; Rosa *et al.* 2015; Wang *et al.* 2015a, 2015b; Zhu *et al.* 2015). Among these methods, adsorption has been recognized as the most attractive process for dye removal from aqueous solution due to its easy operation, high performance and low cost. The effectiveness and efficiency of the adsorbent is the decisive factor for the adsorption technique. Many adsorbents including both synthetic and natural materials, such as

doi: 10.2166/wrd.2016.164

activated carbon, chitosan, agricultural wastes, lignite, sepiolite and so on, have been tested to remove dyes from their aqueous solutions (Dogan *et al.* 2009; Dotto *et al.* 2014; Gürses *et al.* 2014; Zarezadeh-Mehrizi & Badiei 2014; Aboua *et al.* 2015; Duman *et al.* 2015).

Bentonite is an attractive adsorbent due to its advantages such as large specific surface area, good cation exchange capacity and excellent chemical and physical stability (Zaghouane-Boudiaf *et al.* 2014), and it has been used successfully in water treatment as an adsorbent to remove many pollutants such as heavy metals, organic compounds and viruses (Anirudhan & Suchithra 2010; Toor & Jin 2012; Jovic-Jovicic *et al.* 2013; Zha *et al.* 2013; Hao *et al.* 2014; Okabe *et al.* 2014; Bellou *et al.* 2015). In China, use of bentonite as an adsorbent for water purification is of particular convenience as a result of its largest proven reserve of 5,087 million tons and annual production of more than 3.5 million tons in the world. However, natural bentonite has poor capacity for adsorption of anionic dyes because its negatively charged surface, resulting from the isomorphous substitution of Al^{3+} for Si^{4+} in its tetrahedral layer, and Mg^{2+} for Al^{3+} in the octahedral layer, repulses the dye molecule with the same charge in solution (Özer Gök *et al.* 2010; Toor & Jin 2012). Hence, modification of bentonite is very important to improve its adsorption of anionic dyes.

In this work, polyaniline/bentonite composite was synthesized chemically to improve the adsorption capacity of raw bentonite. An anionic dye, reactive green 19 (RG-19), was selected as a target pollutant to test the adsorption characteristics of the polyaniline/bentonite. The effects of various factors including pH, reaction time, temperature and inorganic salts etc. were investigated.

MATERIALS AND METHODS

Preparation of adsorbent

The adsorbent used in this study was synthesized in a manner developed from the modification of the methods described in the published documents Linares & Torres (2005), Motawie *et al.* (2014) and Yapara *et al.* (2005). The specific steps are detailed as follows.

Purified bentonite

The mixture of raw bentonite powder purchased from Inner Mongolia, China, and deionized water was stirred at 4,000 rpm for 0.5 h and then treated by ultrasonic wave for another 0.5 h. The upper layer of the mixture after settlement for 10 min was moved into a beaker and settled for another 24 h. The suspension in the beaker was collected, centrifuged and dried to get the purified bentonite (Puri-Bent).

Sodium bentonite

The sodium bentonite was prepared by dispersing the purified bentonite into 4 wt% Na_2CO_3 solution, followed by being mixed at 80 °C for 2 h. The mixture was then centrifuged and the deposit was washed with deionized water until free of Na_2CO_3, dried at 105 °C, and ground.

Organo-bentonite

The sodium bentonite was dispersed in 20 wt% hexadecyl trimethyl ammonium bromide solution, treated with ultrasonic wave for 30 min, and mixed at 70 °C for 2 h in sequence. The mixture was centrifuged and the deposit was washed with deionized water until free of bromide, dried at 80 °C for 12 h, and ground.

Polyaniline/bentonite

The organo-bentonite was mixed with aniline at the ratio of 1:4 (W:W) for 72 h. The mixture was centrifuged and washed with deionized water until free of aniline and then dried at 80°C for 12 h to get the aniline/bentonite. A total of 5 g of aniline/bentonite was mixed with 20 ml of deionized water containing 50 mg of cyclohexanone peroxide and 2.5 mg of cobalt iso-octoate. The mixture was stirred in an ice bath for 0.5 h and then washed with deionized water, dried and ground to get the polyaniline/bentonite (Pani-Bent).

Characterization of the adsorbent

X-ray diffraction (XRD) and Fourier transform infrared spectroscopy (FTIR) were used to characterize the adsorbent

(Bober *et al.* 2010). XRD patterns of the Puri-Bent and Pani-Bent were acquired with an X-ray diffractometer (X'TRA, ARL Co. Ltd, Switzerland) over the scanning range of $2\theta = 2^\circ - 80^\circ$ to study the changes in their structural properties. Bragg's law $n\,\lambda = 2d\,\sin\theta$ was used to calculate the d_{001} of the two samples. FTIR spectra were obtained by using a FTIR Spectrum (Nicolet 5700, Thermo Nicolet Ltd, USA) to observe the surface functional groups of the two samples.

Preparation of artificial wastewater

RG-19 (chemical formula: $C_{40}H_{23}Cl_2N_{15}Na_6O_{19}S_6$, molecular weight: 1418.93 g mol^{-1}) purchased via the internet was used without further purification. Its structure is shown in Figure 1. The RG-19 solution used in this study was prepared by adding a certain amount of RG-19 into distilled water. The pH value of the dye-containing solution was adjusted with 0.1 M NaOH and 0.1 M HCl solutions and measured using a pH meter (pHS-3C, Leici Ltd, China). All the reagents used were of analytical grade.

Adsorption experiments

The batch RG-19 adsorption experiments were carried out in 100 mL stoppered conical flasks. The flasks filled with 0.1 g of Pani-Bent and 20 mL of RG-19 solution were shaken at a speed of 130 rpm over a period of time at a certain temperature in a shaker. At the end of the adsorption experiments, the solutions were centrifuged at 8,000 rpm for 10 min. The RG-19 concentration in supernatant was measured using an ultraviolet-visible spectrophotometer at the wavelength of maximum absorbance of 630 nm (UV-5100, Yuanxi Instruments, Shanghai, China) (Zuorro *et al.* 2013; Petrucci *et al.* 2015). The RG-19 adsorption by Pani-Bent was calculated by the following Equation (1):

$$q = \frac{(C_0 - C_e)V}{m} \tag{1}$$

where q is the mass of RG-19 adsorbed per unit Pani-Bent (mg/g); C_0 and C_e (mg/L) are the initial and final RG-19 concentration, respectively; V (L) is the volume of RG-19 solution; and m is the weight of Pani-Bent (g).

Statistical analysis

The statistical analysis of the experimental data was conducted by means of a t test using SPSS (Version 17.0, IBM). The confidence level for statistical significance was 95%.

RESULTS AND DISCUSSION

Characterization of adsorbent

The FTIR spectra of Puri-Bent and Pani-Bent were recorded in the range of 4,000–400 cm^{-1} to prove the existence of surface functional groups. As is shown in Figure 2, Puri-Bent and Pani-Bent have a lot of the same groups. For example, absorbed water contributes to O-H stretching at around 3,700, 3,620 and 3,420 cm^{-1}. The band at 1,033 cm^{-1} is due to the Si-O stretching (Saikia & Parthasarathy 2010). The band at 912 cm^{-1} is attributed to Si-O stretching of the silanol group. The bands at 792, 752 and 696 cm^{-1} are due to the mixed Si-O deformations and octahedral sheet vibrations (Quintelas *et al.* 2011). The bands at 536 and 469 cm^{-1} are ascribed to the Si-O-Al stretching and Si-O-Si bending (Saikia & Parthasarathy 2010). Compared with the Puri-Bent spectrum, two new peaks at 2,930 cm^{-1} and 2,850 cm^{-1}, which are assigned to the C-H stretching of alkanes, appear in the Pani-Bent spectrum. The bands at 1,493 and 1,636 cm^{-1} are attributed to ring

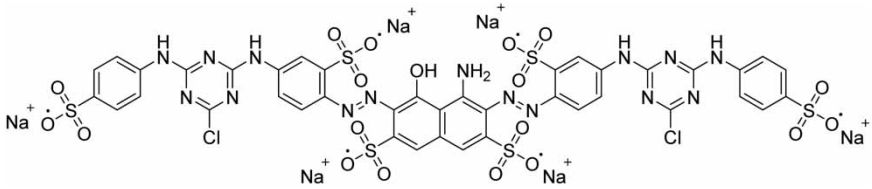

Figure 1 | Chemical structure of RG-19.

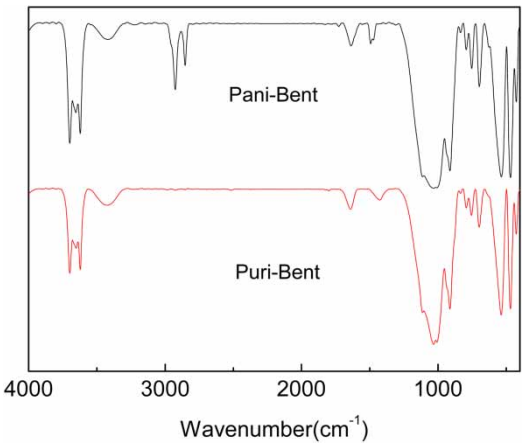

Figure 2 | FTIR spectra of the Puri-Bent and Pani-Bent.

stretching vibration of benzenoid and C = C stretching in aromatic nuclei (Sanches *et al.* 2011; Vivekanandan *et al.* 2011), indicating the successful modification of the raw bentonite.

Figure 3 shows the XRD patterns of Puri-Bent and Pani-Bent. The d_{001} reflection at 2θ for Puri-Bent is 5.98 °, and the corresponding interlayer spacing is 14.77 Å. The 2θ of d_{001} reflection shifts to 5.66° for the Pani-Bent, and its interlayer spacing increases to 15.61 Å. Hence, XRD analyses results indicate that pani molecules did not enter adequately into the layers of bentonite structures.

Effect of pH

Solution pH can affect both the surface charges of the adsorbent and existing forms of dye molecules, which in turn affects the adsorption capacity (Wu *et al.* 2007; Zhang *et al.* 2014). Hence, the effect of pH on RG-19 uptake was investigated. The pH range set for the experiments was 5–9. Theoretically, the interactions caused by electrostatic forces between the negatively charged RG-19 molecules and positively charged active sites on the Puri-Bent surface are the main mechanism for the dye adsorption process, and the adsorption would be weakened with the increasing pH due to the fact that the negative charge of RG-19 and positive charge on the Puri-Bent surface decrease with rising pH. Also, the competition for the active sites between the dye molecule and OH^- in solution causes an adsorption decrease as well. Figure 4 shows RG-19 adsorption decreases from 42.8 to 40.6 mg g^{-1} as the solution pH increases from 5 to 9. Though the overall trend of RG-19 adsorption decreases with the rising pH from 5 to 9, the statistical result shows there is no significant difference in RG-19 uptakes between two adjacent pH values ($p>0.05$), indicating that a slight pH increase leads to a mild decrease in RG-19 adsorption by Pani-Bent in the pH range of 5–9. The same trend was observed when the bentonite modified with hexadecyltrimethylammonium was used to treat reactive black 5 (Jovic-Jovicic *et al.* 2013).

Effect of inorganic salts

During the dyeing process using reactive dyes, inorganic salts are often added to improve dye-fiber bonding by driving the dye molecules out of solution onto the fiber. Therefore,

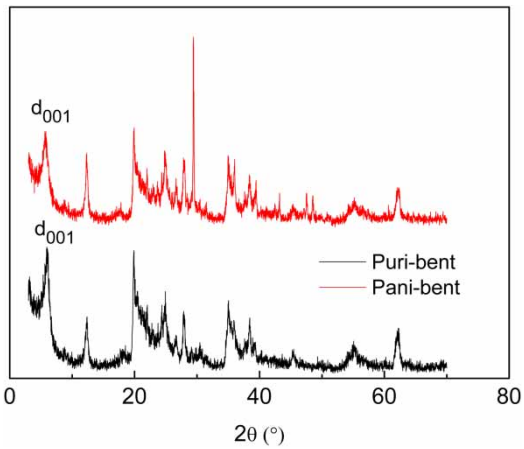

Figure 3 | XRD patterns of the Puri-Bent and Pani-Bent.

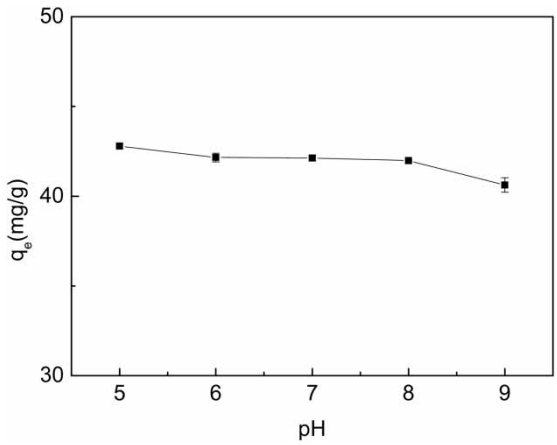

Figure 4 | Effect of pH on RG-19 adsorption by Pani-Bent ($C_0 = 250$ mg/L, T = 25 °C, time = 24 h, pH = 5.9 ± 0.1).

two inorganic salts, NaCl and Na_2SO_4, which are widely used in the dyeing process, were adopted to test their effects on RG-19 adsorption (Figure 5). The RG-19 uptake increases from 42.2 mg g^{-1} without salt to 45.3 mg g^{-1}, 46.8 mg g^{-1} and 48.2 mg g^{-1} by addition of NaCl at doses of 4 g L^{-1}, 8 g L^{-1} and 12 g L^{-1}, respectively. When Na_2SO_4 is used at the same dose, the corresponding RG-19 adsorption is 42.7, 44.5 and 45.8 mg g^{-1}. The results suggest that both NaCl and Na_2SO_4 can improve the RG-19 adsorption at all the three dosages, and the dye adsorption increases significantly with a rising dosage ($p < 0.05$). This result is similar to the removal of reactive black 5 by carbon F400, two bamboo based active carbons and peat reported by Ip *et al.* (2009); however, it is opposite to the adsorption removal of three reactive dyes by metal hydroxide sludge reported by Netpradit *et al.* (2004).The reason why the two salts can promote dye uptake is that the increased intermolecular forces, including van der Waals forces, ion-dipole forces and dipole-dipole forces, induced by the addition of the two inorganic salts prompt the aggregation of dye molecules, which in turn leads to the increase in the extent of RG-19 adsorption on the Pani-Bent surface (Al-Degs *et al.* 2008).

Adsorption kinetics

The effect of reaction time on RG-19 removal is shown in Figure 6. The fast adsorption of RG-19 by Pani-Bent takes place within the first 15 min. This phenomenon may be

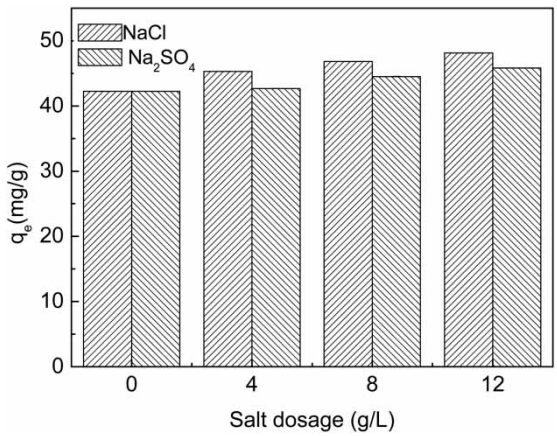

Figure 5 | Effect of inorganic salts on RG-19 adsorption by Pani-Bent ($C_0 = 250$ mg/L, T = 25 °C, time = 24 h, pH = 5.9 ± 0.1).

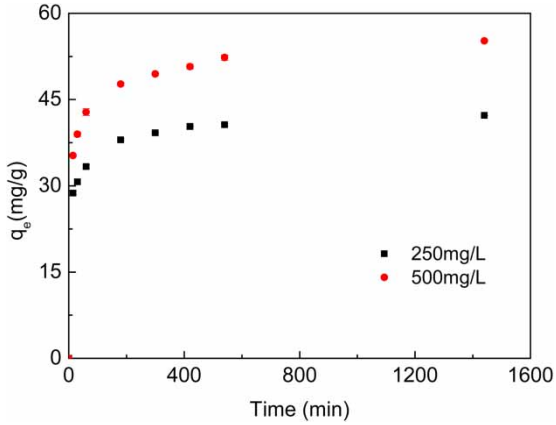

Figure 6 | Effect of reaction time on RG-19 adsorption by Pani-Bent (T = 25 °C, pH = 5.9 ± 0.1).

due to the fact that there are a large numbers of vacant active sites on the surface of Pani-Bent in the initial stage. The adsorption speed increases slowly until practically at equilibrium in 1,440 min, because fewer sites are available in the slow stage and the repulsive forces between the molecules absorbed on the surface of Pani-Bent and the free dye molecules in solution become stronger (Zhang *et al.* 2014).

In order to investigate the adsorption processes of RG-19 by Pani-Bent, adsorption kinetic models including pseudo-first-order, pseudo-second-order and Elovich diffusion equations were adopted (Liu & Zhang 2015). The respective linear forms of the three equations are expressed as Equations (2)–(4):

$$\ln(q_e - q_t) = \ln q_e - k_1 t \tag{2}$$

$$\frac{t}{q_t} = \frac{t}{q_e} + \frac{1}{k_2 q_e^2} \tag{3}$$

$$q_t = \frac{1}{\beta}\ln(\alpha\beta) + \frac{1}{\beta}\ln t \tag{4}$$

where q_t and q_e (mg g^{-1}) are the amount of RG-19 adsorbed at time t and at equilibrium; k_1 (min^{-1}) and k_2 (g mg^{-1} min^{-1}) are the equilibrium rate constants of the pseudo-first-order equation and pseudo-second-order equation, respectively; α (mg g^{-1} min^{-1}) is the initial adsorption rate; and β (g mg^{-1}) is the desorption constant. The two rate constants can be calculated from the plot of experimental data.

The kinetic parameters obtained from the three equations are shown in Table 1. The value of the correlation coefficient R^2 of the pseudo-second-order model is highest among the three coefficients. The $q_{e,cal}$ (41.32 mg g^{-1} for 250 mg L^{-1}, 52.91 mg g^{-1} for 500 mg L^{-1}) calculated from the equations agree very well with $q_{e,\ exp}$ (42.24 mg g^{-1} for 250 mg L^{-1}, 55.23 mg g^{-1} for 500 mg L^{-1}) obtained from the experiments. As a result, the pseudo-second-order model is best suited to describe the adsorption process of RG-19 by Pani-Bent. The results suggest that the chemical adsorption or chemisorption might be the rate determining step, and the valency forces through sharing or exchange of electrons between the dye molecules and the active sites of the Pani-Bent adsorbate might be involved in the reaction (Örnek *et al.* 2007).

Adsorption isotherm studies

The adsorption isotherm gives an idea of the distribution of the adsorbate molecules between the liquid-solid interface when the adsorption reaches its equilibrium, and adsorption parameters can be also obtained by analysis of isotherm data (Peng *et al.* 2005; Hameed *et al.* 2008). So, two widely used isotherm equations, the Langmuir and Freundlich models, were used to fit the data obtained from the experiments. The linear forms of the two models are expressed as Equations (5) and (6):

$$\frac{C_e}{q_e} = \frac{1}{q_m b} + \frac{C_e}{q_m} \tag{5}$$

$$\log q_e = \log k_f + \frac{1}{n}\log C_e \tag{6}$$

Table 1 | Parameters of the three kinetic equations for RG-19 adsorption by Pani-Bent

Kinetics equations	Parameters	250 mg L^{-1}	500 mg L^{-1}
Pseudo-first-order	q_e	16.40	23.09
	k_1	0.005	0.004
	R^2	0.820	0.805
Pseudo-second-order	q_e	41.32	52.91
	k_2	0.002	0.001
	R^2	0.997	0.999
Elovich	α	1870.7	1039.1
	β	0.313	0.227
	R^2	0.977	0.992

where q_e (mg g^{-1}) is the amount of RG-19 adsorbed per unit mass of Pani-Bent; C_e (mg L^{-1}) is the RG-19 concentration at equilibrium; q_m (mg g^{-1}) is the maximum adsorption capacity; b (L mg^{-1}) is the Langmuir constant related to binding energy; and K_f and n are the Freundlich constants related to adsorption capacity and adsorption intensity, respectively.

The adsorption isotherms are presented in Figure 7, and the calculated constants of the two models are shown in Table 2. The correlation coefficients R^2 of the Langmuir model are higher than those of the Freundlich model, indicating the Langmuir model fits the data better than the Freundlich model. R_L, a dimensionless constant separation factor was used to further understand the characteristic of the adsorption process. The factor is defined as Equation (7):

$$R_L = \frac{1}{1 + bC_0} \tag{7}$$

where C_0 (mg L^{-1}) is the initial RG-19 concentration; and b (L mg^{-1}) is the Langmuir adsorption equilibrium constant.

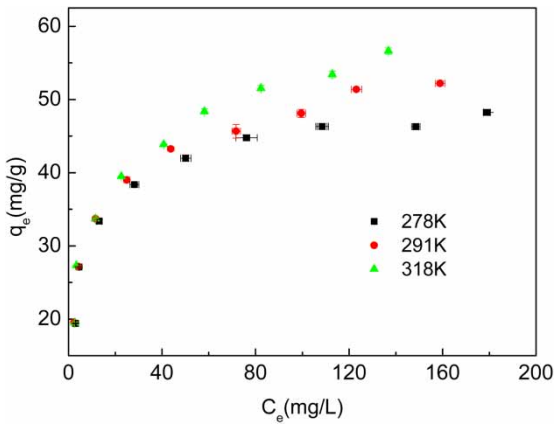

Figure 7 | Adsorption isotherms of RG-19 by Pani-Bent at three temperatures (time = 24 h, pH = 5.3 ± 0.2).

Table 2 | Adsorption isotherm constants for adsorption of RG-19 by Pani-Bent

	Langmuir			Freundlich		
T(K)	R^2	q_m	b	R^2	n	k_f
278	0.999	49.02	0.162	0.919	5.102	3.558
291	0.997	53.48	0.135	0.959	4.717	3.567
318	0.995	58.14	0.118	0.956	4.241	3.527

Table 3 | R_L values based on the Langmuir model

	R_L								
T(K)	100 mg L^{-1}	140 mg L^{-1}	180 mg L^{-1}	220 mg L^{-1}	260 mg L^{-1}	300 mg L^{-1}	340 mg L^{-1}	380 mg L^{-1}	420 mg L^{-1}
278	0.058	0.040	0.033	0.027	0.023	0.020	0.017	0.016	0.014
291	0.993	0.050	0.040	0.033	0.028	0.024	0.021	0.019	0.017
318	0.895	0.960	0.960	0.970	0.974	0.977	0.980	0.982	0.983

The values of R_L calculated for different initial concentrations at different temperatures are given in Table 3. The fact that $0 < R_L < 1$ for all of the experiments indicates the favorable nature of the adsorption of RG-19 by Pani-Bent.

Thermodynamics

Thermodynamic parameters of the adsorption were calculated using Equations (8) and (9) (Tütem *et al.* 1998; Huang *et al.* 2007; Shao *et al.* 2012).

$$\Delta G^\circ = \Delta H^\circ - T\Delta S^\circ \tag{8}$$

$$\ln C_e = \left(\ln q_e - \frac{\Delta S^\circ}{R}\right) + \frac{\Delta H^\circ}{R}\frac{1}{T} \tag{9}$$

where q_e (mg g^{-1}) and C_e (mg L^{-1}) are the amount of RG-19 adsorbed per unit mass of Pani-Bent, and RG-19 concentration at equilibrium, respectively. ΔH° (kJ mol^{-1}), ΔS° (kJ K^{-1} mol^{-1}) and ΔG° (kJ mol^{-1}) are the enthalpy, entropy and the standard Gibbs free energies, respectively. R (8.314 J mol^{-1} K^{-1}) is the ideal gas constant, and T (K) is the temperature in Kelvin.

The values of C_e are calculated using the method of Tütem *et al.* (1998). ΔH° and ΔS° are obtained from the slopes and intercepts of the plots of $\ln C_e$ vs. $1/T$ (Figure 8). The values of ΔG° are calculated from Equation (8). The thermodynamic parameters including ΔH°, ΔS° and ΔG° are listed in Table 4. The negative values of ΔG° indicate the feasibility of the process and the spontaneous nature of the adsorption. The decreasing ΔG° with the rising temperature indicates better adsorption at higher temperature (Chen & Wang 2006). The positive values of ΔH° indicate the adsorption is endothermic.

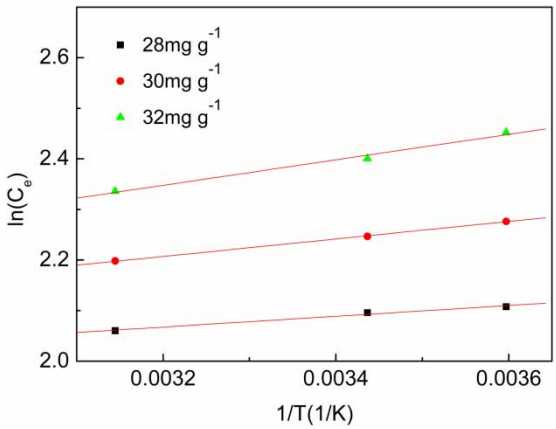

Figure 8 | Plots of $\ln C_e$ versus $1/T$ for adsorption of RG-19 by Pani-Bent.

Table 4 | Thermodynamic parameters for RG-19 adsorption by Pani-Bent

			ΔG° (kJ mol^{-1})		
Q_e (mg g^{-1})	ΔH° (kJ mol^{-1})	ΔS° (J K^{-1} mol^{-1})	278 K	291 K	318 K
28	0.887	0.013	−2.825	−2.999	−3.360
30	1.438	0.015	−2.601	−2.790	−3.182
32	2.094	0.016	−2.353	−2.561	−2.993

CONCLUSIONS

The Pani-Bent was synthesized, characterized and used for RG-19 removal in this study. The RG-19 uptake decreased slightly with increasing solution pH. Both NaCl and Na_2SO_4 increased the dye adsorption with rising salt dosage, resulting from aggregation of the dye molecules in solution. The kinetic data fitted the pseudo-second-order kinetic model best among the three models, and isotherm data were described better by the Langmuir model than by the Freundlich model. Adsorption of RG-19 was found to be spontaneous and endothermic at the temperature range

of 278–328 K in this study, as indicated from the negative values of ΔG° and ΔH°. The results indicated that the Pani-Bent is an effective adsorbent for anionic dye removal from water.

REFERENCES

Aboua, K. N., Yobouet, Y. A., Yao, K. B., Goné, D. L. & Trokourey, A. 2015 Investigation of dye adsorption onto activated carbon from the shells of Macoré fruit. *J. Environ. Manag.* **156**, 10–14.

Al-Degs, Y. S., El-Barghouthi, M. I., El-Sheikh, A. H. & Walker, G. M. 2008 Effect of solution pH, ionic strength, and temperature on adsorption behavior of reactive dyes on activated carbon. *Dyes Pigments* **77**, 16–23.

Anirudhan, T. S. & Suchithra, P. S. 2010 Heavy metals uptake from aqueous solutions and industrial wastewaters by humic acid-immobilized polymer/bentonite composite: kinetics and equilibrium modeling. *Chem. Eng. J.* **156**, 146–156.

Bellou, M. I., Syngouna, V. I., Tselepi, M. A., Kokkinos, P. A., Paparrodopoulos, S. C., Vantarakis, A. & Chrysikopoulos, C. V. 2015 Interaction of human adenoviruses and coliphages with kaolinite and bentonite. *Sci. Total. Environ.* **517**, 86–95.

Bober, P., Stejskal, J., Spírková, M., Trchová, M., Varga, M. & Prokeš, J. 2010 Conducting polyaniline–montmorillonite composites. *Synthetic Met.* **160**, 2596–2604.

Chen, C. L. & Wang, X. K. 2006 Adsorption of Ni(II) from aqueous solution using oxidized multiwall carbon nanotubes. *Ind. Eng. Chem. Res.* **45**, 9144–9149.

Dogan, M., Abak, H. & Alkan, M. 2009 Adsorption of methylene blue onto hazelnut shell: kinetics, mechanism and activation parameters. *J. Hazard. Mater.* **164**, 172–181.

Dotto, G. L., Buriol, C. & Pinto, L. A. A. 2014 Diffusional mass transfer model for the adsorption of food dyes on chitosan films. *Chem. Eng. Res. Des.* **92**, 2324–2332.

Duman, O., Tunç, S. & Polat, T. G. 2015 Adsorptive removal of triarylmethane dye (Basic Red 9) from aqueous solution by sepiolite as effective and low-cost adsorbent. *Micropor. Mesopor. Mat.* **210**, 176–184.

Ewa, L. G. & Gra, G. 2007 Adsorption characteristics of Congo Red on coal-based mesoporous activated carbon. *Dyes Pigments* **74**, 34–40.

Gong, J. L., Wang, B., Zeng, G. M., Yang, C. P., Niu, C. G., Niu, Q. Y., Zhou, W. J. & Liang, Y. 2009 Removal of cationic dyes from aqueous solution using magnetic multi-wall carbon nanotube nanocomposite as adsorbent. *J. Hazard. Mater.* **164**, 1517–1522.

Gürses, A., Hassani, A., Kıranşan, M., Açışlı, Ö. & Karaca, S. 2014 Removal of methylene blue from aqueous solution using by untreated lignite as potential low-cost adsorbent: kinetic, thermodynamic and equilibrium approach. *J. Water Process Eng.* **2**, 10–21.

Hameed, B. H., Tan, I. A. W. & Ahmad, A. L. 2008 Adsorption isotherm, kinetic modeling and mechanism of 2,4,6-trichlorophenol on coconut husk-based activated carbon. *Chem. Eng. J.* **144**, 235–244.

Hao, Y. F., Yan, L. G., Yu, H. Q., Yang, K., Yu, S. J., Shan, R. R. & Du, B. 2014 Comparative study on adsorption of basic and acid dyes by hydroxy-aluminum pillared bentonite. *J. Mol. Liq.* **199**, 202–207.

Hua, X., Teng, F., Zhao, Y. X., Xu, J., Xu, C. Y., Yang, Y., Zhang, Q. Q., Paul, S. S., Zhang, Y., Chen, M. D. & Zhao, X. D. 2015 A new application of high-efficient silver salts-based photocatalyst under natural indoor weak light for wastewater cleaning. *Water Res.* **81**, 366–374.

Huang, J. H., Liu, Y. F., Jin, Q. Z., Wang, X. G. & Yang, J. 2007 Adsorption studies of a water soluble dye, Reactive Red MF-3B, using sonication-surfactant-modified attapulgite clay. *J. Hazard. Mater.* **143**, 541–548.

Ip, A. W., Barford, J. P. & McKay, G. 2009 Reactive Black dye adsorption/desorption onto different adsorbents: effect of salt, surface chemistry, pore size and surface area. *J. Colloid Interf. Sci.* **337**, 32–38.

Jovic-Jovicic, N. P., Milutinovic-Nikolic, A. D. & Zunic, M. J. 2013 Synergic adsorption of Pb^{2+} and reactive dye–RB5 on two series of organomodified bentonites. *J. Contam. Hydrol.* **150**, 1–11.

Kim, H., Kang, S. O., Park, S. & Park, H. S. 2015 Adsorption isotherms and kinetics of cationic and anionic dyes on three-dimensional reduced graphene oxide macrostructure. *J. Ind. Eng. Chem.* **25**, 1191–1196.

Liang, C. Z., Sun, S. P., Li, F. Y., Ong, Y. K. & Chung, T. S. 2014 Treatment of highly concentrated wastewater containing multiple synthetic dyes by a combined process of coagulation/flocculation and nanofiltration. *J. Membrane Sci.* **469**, 306–315.

Linares, C. F. & Torres, A. 2005 Modified bentonite with Na_2CO_3 as possible antacid medicament. *Stud. Surf. Sci. Catal.* **B158**, 1073–1080.

Liu, X. & Zhang, L. F. 2015 Removal of phosphate anions using the modified chitosan beads: adsorption kinetic, isotherm and mechanism studies. *Powder Technol.* **277**, 112–119.

Mahmoodi, N. M. 2013 Photocatalytic ozonation of dyes using multiwalled carbon nanotube. *J. Mol. Catal. A-Chem.* **366**, 254–260.

Motawie, A. M., Madany, M. M., El-Dakrory, A. Z., Osman, H. M., Ismail, E. A., Badr, M. M., El-Komy, D. A. & Abulyazied, D. E. 2014 Physico-chemical characteristics of nano-organo bentonite prepared using different organo-modifiers. *Egypt. J. Petrol.* **23**, 331–338.

Netpradit, S., Thiravetyan, P. & Towprayoon, S. 2004 Adsorption of three azo reactive dyes by metal hydroxide sludge: effect of temperature, pH, and electrolytes. *J. Colloid. Interf. Sci.* **270**, 255–261.

Okabe, R., Miura, A., Fukushima, M., Terashima, M., Sasaki, M., Fukuchi, S. & Sato, T. 2014 Adsorption of pentachlorophenol to a humin-like substance-bentonite complex prepared by

polycondensation reactions of humic precursors. *Appl. Clay Sci.* **87**, 136–141.

Ong, S. A., Min, O. M., Ho, L. N. & Wang, Y. S. 2013 Solar photocatalytic degradation of mono azo methyl orange and diazo reactive green 19 in single and binary dye solutions: adsorbability vs photodegradation rate. *Environ. Sci. Pollut. Res.* **20**, 3405–3413.

Örnek, A., Özacar, M. & Şengil, İ. A. 2007 Adsorption of lead onto formaldehyde or sulphuric acid treated acorn waste: equilibrium and kinetic studies. *Biochem. Eng. J.* **37**, 192–200.

Özer Gök, A., Özcan, S. & Özcan, A. 2010 Adsorption behavior of a textile dye of Reactive Blue 19 from aqueous solutions onto modified bentonite. *Appl. Surface Sci.* **256**, 5439–5443.

Peng, Z. G., Hidajat, K. & Uddin, M. S. 2005 Selective and sequential adsorption of bovine serum albumin and lysozyme from a binary mixture on nanosized magnetic particles. *J. Colloid Interf. Sci.* **281**, 11–17.

Peng, L. H., Zhang, Y. T., Wang, Y. J., Zeng, X. L., Peng, N. J. & Yu, A. 2015 Energy efficiency and influencing factor analysis in the overall Chinese textile industry. *Energy* **93**, 1222–1229.

Petrucci, E., Palma, L., Lavecchia, R. & Zuorro, A. 2015 Modeling and optimization of Reactive Green 19 oxidation on a BDD thin-film electrode. *Taiwan Ins. Chem. Eng.* **51**, 152–158.

Quintelas, C., Figueiredo, H. & Tavares, T. 2011 The effect of clay treatment on remediation of diethylketone contaminated wastewater: uptake, equilibrium and kinetic studies. *J. Hazard. Mater.* **186**, 1241–1248.

Rosa, J. M., Tambourgi, E. B., Santana, J. C. C., Araujo, M. C., Ming, W. C. & Trindade, N. 2014 Development of colors with sustainability: a comparative study between dyeing of cotton with reactive and vat dyestuffs. *Text. Res. J.* **84**, 1009–1017.

Rosa, J. M., Fileti, A. M. F., Tambourgi, E. B. & Santana, J. C. C. 2015 Dyeing of cotton with reactive dyestuffs: the continuous reuse of textile wastewater effluent treated by Ultraviolet/Hydrogen peroxide homogeneous photocatalysis. *J. Cleaner Prod.* **90**, 60–65.

Saikia, B. J. & Parthasarathy, G. 2010 Fourier transform infrared spectroscopic characterization of kaolinite from Assam Meghalaya, Northeastern India. *J. Mod. Phys.* **1**, 206–210.

Sanches, E. A., Soares, J. C., Iost, R. M., Marangoni, V. S., Trovati, G., Batista, T., Mafud, A. C., Zucolotto, V. & Mascarenhas, Y. P. 2011 Structural characterization of emeraldine-salt polyaniline/gold nanoparticles complexes. *J. Nanomater.* **2011**, 1–7.

Shao, L., Ren, Z., Zhang, G. & Chen, L. 2012 Facile synthesis, characterization of a $MnFe_2O_4$/activated carbon magnetic composite and its effectiveness in tetracycline removal. *Mat. Chem. Phys.* **135**, 16–24.

Tang, L., Cai, Y., Yang, G., Liu, Y., Zeng, G., Zhou, Y., Li, S., Wang, J., Zhang, S., Fang, Y. & He, Y. 2014 Cobalt nanoparticles-embedded magnetic ordered mesoporous carbon for highly effective adsorption of rhodamine B. *Appl. Surface Sci.* **314**, 746–753.

Toor, M. & Jin, B. 2012 Adsorption characteristics, isotherm, kinetics, and diffusion of modified natural bentonite for removing diazo dye. *Chem. Eng. J.* **187**, 79–88.

Tütem, E., Apak, R. & Ünal, Ç. F. 1998 Adsorptive removal of chlorophenols from water by bituminous shale. *Water Res.* **32**, 2315–2324.

Vivekanandan, J., Ponnusamy, V., Mahudeswaran, A. & Vijayanand, P. S. 2011 Synthesis, characterization and conductivity study of polyaniline prepared by chemical oxidative and electrochemical methods. *Arch. Appl. Sci. Res.* **3**, 147–153.

Wang, L. & Wang, A. Q. 2008 Adsorption behaviors of Congo Red on the N,O-carboxymethyl-chitosan/ montmorillonite nanocomposite. *Chem. Eng. J.* **143**, 43–50.

Wang, J. D., Yan, J. J. & Xu, W. J. 2015a Treatment of dyeing wastewater by MIC anaerobic reactor. *Biochem. Eng. J.* **10**, 179–184.

Wang, Y. G., Yao, M. C., Chen, Y. T., Zuo, Y. H., Zhang, X. D. & Cui, L. F. 2015b General synthesis of magnetic mesoporous FeNi/graphitic carbon nanocomposites and their application for dye adsorption. *J. Alloycompd.* **627**, 7–12.

Wu, X. B., Wu, D. C. & Fu, R. W. 2007 Studies on the adsorption of reactive brilliant red X-3B dye on organic and carbon aerogels. *J. Hazard. Mater.* **147**, 1028–1036.

Yapara, S., Özbudak, V., Dias, A. & Lopes, A. 2005 Effect of adsorbent concentration to the adsorption of phenol on hexadecyl trimethyl ammonium-bentonite. *J. Hazard. Mater* **B121**, 135–139.

Zaghouane-Boudiaf, H., Boutahala, M., Sahnoun, S., Tiar, C. & Gomri, F. 2014 Adsorption characteristics, isotherm, kinetics, and diffusion of modified natural bentonite for removing the 2,4,5-trichlorophenol. *Appl. Clay Sci.* **90**, 81–87.

Zarezadeh-Mehrizi, M. & Badiei, A. 2014 Highly efficient removal of basic blue 41 with nanoporous silica. *Water Resour. Ind.* **5**, 49–57.

Zha, S. X., Zhou, Y., Jin, X. Y. & Chen, Z. L. 2013 The removal of amoxicillin from wastewater using organobentonite. *J. Environ. Manage.* **129**, 569–576.

Zhang, X. B., Dong, W. Y. & Yang, W. 2013 Decolorization efficiency and kinetics of typical reactive azo dye RR2 in the homogeneous Fe(II) catalyzed ozonation process. *Chem. Eng. J.* **233**, 14–23.

Zhang, C., Yang, S. G., Chen, H. Z., He, H. & Sun, C. 2014 Adsorption behavior and mechanism of reactive brilliant red X-3B in aqueous solution over three kinds of hydrotalcite-like LDHs. *Appl. Surface Sci.* **301**, 329–337.

Zhu, J. Y., Tian, M. M., Zhang, Y. T., Zhang, H. Q. & Liu, J. D. 2015 Fabrication of a novel 'loose' nanofiltration membrane by facile blending with Chitosan–Montmorillonite nanosheets for dyes purification. *Chem. Eng. J.* **265**, 184–193.

Zuorro, A., Fidaleo, M. & Lavecchia, R. 2013 Response surface methodology (RSM) analysis of photodegradation of sulfonated diazo dye Reactive Green 19 by UV/H_2O_2 process. *J. Environ. Manage.* **127**, 28–35.

First received 28 September 2015; accepted in revised form 8 December 2015. Available online 8 February 2016